#2001131

Physical property data and geophysical models to accompany “Rooted Brooks Range ophiolite: Implications for Cordilleran terranes” by Saltus, Hudson, Karl, and Morin.

Data Repository

Introduction

This data compilation and summary of geophysical modeling accompanies our report (Saltus et al., 2001) on the implications of a tectonic reinterpretation of the mafic and ultramafic rocks of the Copter Peak and Misheguk Mountain allochthons in the Noatak region of northwestern Alaska. We describe and present magnetic susceptibility and density measurements made on mafic and ultramafic rocks from the study area. We then present a series of magnetic and gravity models to illustrate geophysical constraints on the geological interpretation of these rocks. In contrast with the prevailing geological interpretations for the area, we find that the basalt, gabbro, and ultramafic rocks are thick and intermixed at depth.

New physical property data

Measured and inferred densities and magnetic susceptibilities provide bounds for potential field models of the Copter Peak and Misheguk Mountain allochthons in the Noatak region. Table 1 lists densities and magnetic susceptibilities measured on hand samples collected on and around Asik Mountain in June 2000 (assisted by Gil Mull); sample locations shown are shown on Figures 1 and 2. The samples designated Mv are all from Asik Mountain. Tables 2.1-2.7 contains magnetic susceptibility measurements made by us on alluvial basalt boulders in seven drainages in the Maiyumerak Mountains basalt massif; these measurement locations are shown on Figure 2. Table 3 is a summary of the density and magnetic susceptibility information combined with measurements on rocks from the Siniktanneayak complex (Morin and Moore, 1996) to the northeast and Baird Mountains to the east.

We measured magnetic susceptibilities using a hand-held KAPPAMETER susceptibility meter manufactured by GEOFYZIKA a.s. in the Czech Republic. The meter has a sensitivity of 1×10^{-5} SI. Before every rock measurement the meter was calibrated by taking a free space measurement. The values reported are the apparent susceptibility values direct from the instrument readout. Depending on the size of the rock sample and the surface roughness, these values may underestimate true susceptibility by up to 15%. Care was taken to make measurements on flat surfaces of samples greater than 10 cm in thickness and diameter to minimize this underestimation.

Densities were measured by weighing dry (Wa) and saturated (Ws) rock samples in air and weighing the saturated sample suspended in water (Ww). Weights were measured on a calibrated scale to an accuracy of better than 0.05 gm. Three densities were calculated: (1) grain density = Wa/(Wa-Ww), (2) saturated bulk density = Ws/(Ws-Ww), and (3) dry bulk density = Wa/(Ws-Ww). We used the saturated bulk densities for modeling. Densities are accurate to better than 0.01 g/cm^3.

Our 12 laboratory and over 700 field measurements indicate that the Copter Peak basalts have magnetic susceptibilities ranging from essentially zero to a maximum of about 100 x 10^{-3} SI with an average value of 15 x 10^{-3} SI. Density measurements on 4 basalt samples range from 2.80 to 2.98 g/cm^3 with an average value of 2.85 g/cm^3. Forty-one laboratory magnetic susceptibility measurements on gabbros of the Misheguk Mountain allochthon have values ranging from essentially zero to 113 x 10^{-3} SI with an average of about 35 x 10^{-3} SI. Density measurements on 20 gabbros show a range of 2.82 to 3.22 g/cm^3 with an average of 3.03 g/cm^3. Six laboratory measurements on ultramafic rocks from Asik Mountain show magnetic susceptibilities ranging from 0.6 to 49 x 10^{-3} SI with an average value of 14 x 10^{-3} SI. Eight density measurements on ultramafic rocks from Asik Mountain range from 3.00 to 3.24 g/cm^3 with an average value of 3.18 g/cm^3.

Gravity and magnetic profile models

A series of two-dimensional magnetic and gravity models along aeromagnetic profiles #1 and #2 (Saltus et al., 2001, Figure 2) demonstrate some of the volumetric and structural constraints that these data impose on geologic interpretations of the Copter Peak and Misheguk Mountain allochthons.

Figure G1 shows two models that demonstrate the difficulty of fitting the aeromagnetic data on profile #1 with a **thin, synformal body**. In model 1.1, the best-fitting uniform magnetic susceptibility was calculated for a synformal body with a horizontal base at about 3 km depth. The calculated effect of this body fails to match the observed data in two key ways: (1) the complex shape in the center of the body is not matched, and (2) the flanks of the anomaly are too steep and don't match the smooth flanks of the observed data. In model 1.2 we preserved the thin synformal shape required by previous geologic interpretations and allowed the magnetic susceptibility to vary laterally within steep-sided domains. We used an automatic inversion method to calculate the best-fitting susceptibility values. Even if we allow the susceptibilities to vary freely, the model still fails to match the broad flanks of the observed anomaly. The laterally variable domains do allow us to fit the complex shape of the center of the anomaly, but the susceptibilities required are greater than those we observed in any of our measured rock properties from the region.

Figure G2 shows a series of models that demonstrate the inability to fit the aeromagnetic anomaly on profile #2 with a **uniformly magnetized body**. This series of models were calculated in the pseudogravity domain. The pseudogravity transform (Baranov, 1957) is a mathematical way to convert a magnetic anomaly into a gravity-like anomaly that may be more conducive to interpretation (Blakely, 1995). This technique is advantageous here because: (1) it reduces the sensitivity of the models to shallow effects, and (2) it removes a dependence on magnetic field direction. The appropriate physical property in the pseudogravity domain is pseudodensity. Pseudodensity can be converted mathematically to an equivalent magnetic susceptibility. For each of the 6 uniformly magnetized bodies in figure G2 we label the modeled pseudodensity value (D) and the equivalent susceptibility value (S). The equivalent susceptibilities range from 17 to 112 x 10^{-3} SI. Each of the model bodies extends to the surface. The bottom interface of each body is adjusted to fit the broad northern bulge of the aeromagnetic anomaly. Models 2.1 and 2.2 fit the steep-sided southern high over Asik Mountain but the others do not. Given that the mean measured susceptibility for the Copter Peak basalts is 15 x 10^{-3} SI and that of the Misheguk Mountain gabbros is about 35 x 10^{-3} SI, it is difficult to accept models 2.1 to 2.3 that use average susceptibilities that are 2 to 3 times this amount. The best compromise is perhaps provided by model 2.4 with an assumed susceptibility of 41 x 10^{-3} SI. This model extends to 8 km depth and still fails to match the highest and steepest part of the Asik Mountain high. Model 2.6 is an attempt to fit the anomalies with a uniformly magnetized body with a susceptibility equal to the measured value for the Copter Peak basalts. This produces a body that is significantly thicker than 25 km, and does not provide a good fit to the Asik Mountain high. These modeling results for uniformly magnetized bodies are all unsatisfactory and demonstrate the need for multi-body models to satisfy the geologic, physical property, and aeromagnetic data constraints.

Figure G3 shows several **multi-body models** that illustrate the range of possible geophysical solutions along profile #1. In each case, body A is set to the measured average magnetic susceptibility of the Copter Peak basalts as exposed along this profile. Several scenarios for the susceptibility and shape of the deeper, more highly magnetized body B, are illustrated in the models. In model 3.1 we require the base of body B to be approximately horizontal and allow body B to assume a relatively high susceptibility (nearly twice the average we measured for the Misheguk Mountain gabbro). Model 3.2 shows a scenario in which the bottom of body B is allowed to vary and we flatten the interface between the two source bodies. Model 3.3 shows a model that results if we use the measured average susceptibility of the Misheguk Mountain gabbro for body B. This series of models demonstrates that we can fit the observed anomalies if we place more magnetic rocks beneath the Copter Peak basalts. If these rocks are like the Misheguk Mountain gabbros, the overall assemblage must be quite thick, probably greater than 8 km.

Figure G4 shows two **combined gravity and magnetic models** along profile #2, which crosses the gravity and magnetic high at Asik Mountain. In these models each body is assigned both a magnetic susceptibility and a density value and the calculated effects must match both the observed aeromagnetic and ground-based gravity data. Densities are listed as values (in g/cm^3) relative to the surrounding country rock. To convert to absolute densities, add these values to the assumed background density of 2.7 g/cm^3. To fit the data, we were required to create models with four separate geophysical bodies. In both models, body A has magnetic susceptibility equal to that measured for the Copter Peak basalts, but has a lower density as required by the gravity values in the northern part of the profile. These lower gravity values are partially caused by the affects of low-density sediments in the Noatak basin to the west of the profile. In both models, body B has density and susceptibility values that reflect our measured values for the Copter Peak basalts. To match the Asik Mountain gravity and magnetic highs we were required in both models to include the very magnetic, dense, and shallow body C. This body has magnetic susceptibility at the maximum end of any we measured in the region and a density higher than any we measured. For model 4.1, body D has density and magnetic susceptibility at the upper end of those we measured on gabbros. For model 4.2, body D has density and susceptibilities that reflect the average values we obtained in our measurements. In both models the shape of the bottom of the complex is not well constrained – there are modeling trade-offs with the shape of the interface between bodies B and D – but, the overall thickness is about 8 km. Similarly, in both models a multi-body solution is required to fit all available data.

Conclusions

Analysis of a series of magnetic and gravity models indicates that the Copter Peak basalts are very thick and are underlain by regionally more magnetic and locally more dense rocks. When model susceptibilities and densities are constrained by our measurements on basalt, gabbro, and ultramafic rocks in the region, they produce total thickness for the mafic and ultramafic complex of at least 8 km. There are insufficient additional constraints to produce a single preferred geophysical model for the subsurface character of the basalt, gabbro, and ultramafic rocks but the available data and models that indicate these rocks are thick and intermixed at depth are robust.

References

Baranov, V., 1957, A new method for interpretation of aeromagnetic maps: pseudo-gravimetric anomalies: Geophysics, v. 22, p. 359-383.

Blakely, R.J., 1995, Potential Theory in Gravity and Magnetic Applications: Cambridge University Press, New York, 441 p.

Morin, R.L., and Moore, T.E., 1996, Gravity models of the Siniktanneayak mafic-ultramafic complex, western Brooks Range, Alaska: Evidence for thrust emplacement of Brooks Range ophiolites, *in* Moore, T.E., and Dumoulin, J.A., eds., Geological Studies in Alaska by the U.S. Geological Survey, 1994: U.S. Geological Survey Bulletin 2152, p. 101-110.

Saltus, R.W., Hudson, T.L, Karl, S.M., and Morin, R.L., 2001, Rooted Brooks Range ophiolite: Implications for Cordilleran terranes: Geology, v. XX, n. YY, p. X-Y.

Figure 1 - Asik Mountain sample sites

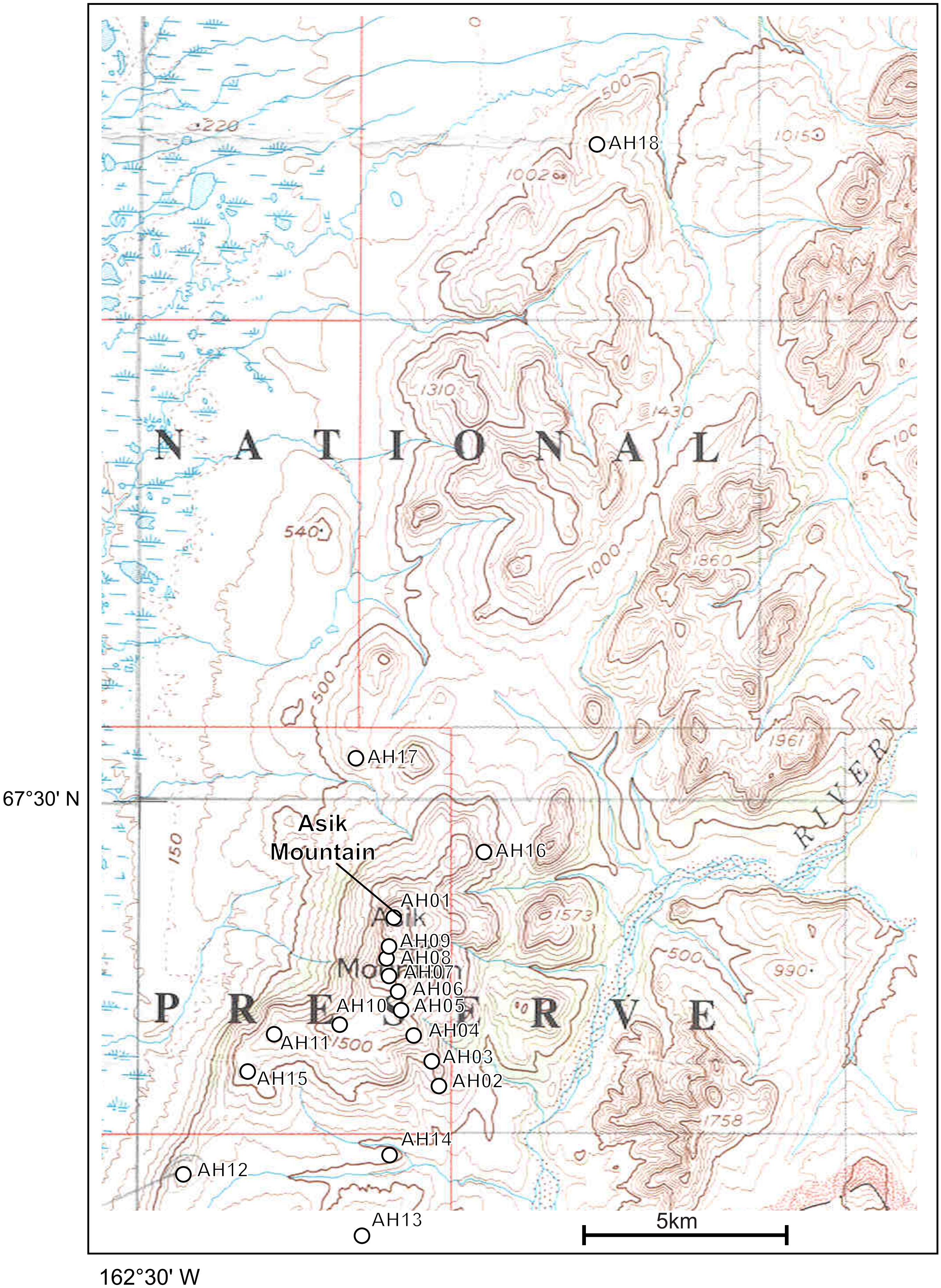

Figure 2 - Maiyumerak Mountains sample sites

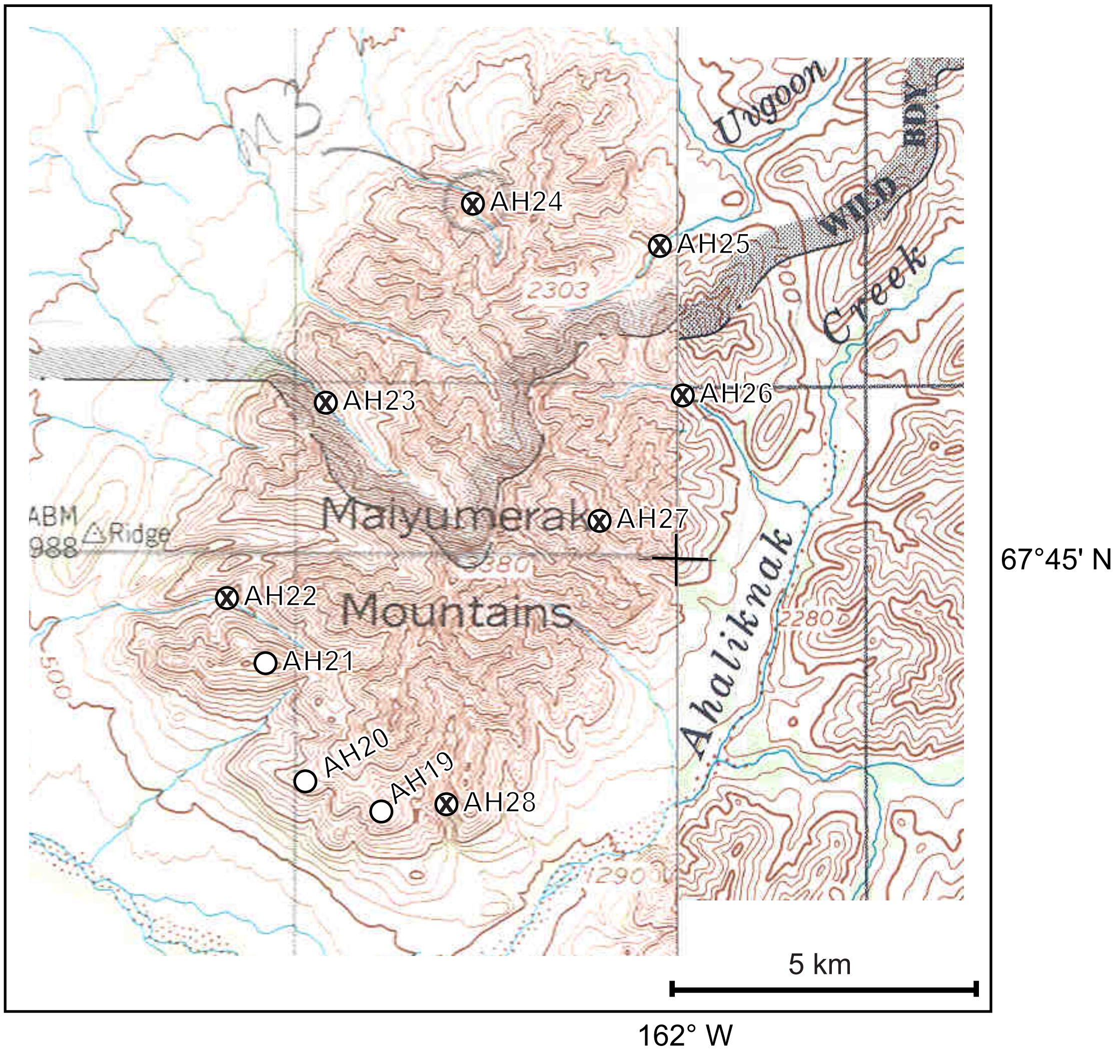

Table 1

Office measured susceptibilities on hand samples from Noatak 2000 fieldtrip
Saltus & Hudson, 11 July 2000

		model susceptibilities			model densities	
Population categories:		SI x 10-3	cgs x 10-3	Inferred lithology(ies)		
dead	<2			metamorphosed gabbros, some basalts	basalt	2.9
low	2<x<10 (mean 5)	5	0.4	most basalts, most umafic	gabbro	3.1
med	10<x<80 (mean 25)	25	2.0	some basalts, some gabbros	umafic	3.2
high	80<x (mean 100)	100	8.0	some gabbros		

									Weights (gm)			Densities (g/cm3)				
									in air	in water	saturated	grain	sat bulk	dry bulk		
Site	Lithology(Travis, Gil)	Mag category	Susceptibilities (SI x 10-3)				SUS MEAN	Site	Wa	Ww	Ws	D1	D2	D3	DEN MEAN	
00AH18	basalt	dead	0.44	0.46				00AH18	193.76	129.19	194.33	3.00	2.98	2.97		
00AH19	basalt	low	2	7	10			00AH19	554.20	355.80	555.39	2.79	2.78	2.78		
00AH19	basalt	dead	0.28	0.04				00AH19								
00AH20	basalt	med	18.7	12.7				00AH20								
00AH20a	basalt						basalt	00AH20a	281.90	183.83	283.22	2.87	2.85	2.84	basalt	
00AH23	basalt	high,med,dead	93.6	40	0.34	ave	15.46	00AH23	392.70	253.85	394.82	2.83	2.80	2.79	2.85	ave
00AH25	basalt & gabbro	med, low	57.3	4.01		stddev	27.23	00AH25							0.09	std dev
00AH20b	diabase					count	12	00AH20b	327.47	213.36	328.42	2.87	2.85	2.85	4	count
00AH01B	gabbro	low	7.75			max	93.60	00AH01B	1240.30	825.52	1242.63	2.99	2.98	2.97		
00AH01b	gabbro	med	17	27.3				00AH01b								
00AH02a	gabbro							00AH02a	402.60	271.37	404.05	3.07	3.05	3.03		
00AH02b	gabbro							00AH02b	446.00	301.77	447.39	3.09	3.07	3.06		
00AH03	gabbro	med, low	25.5	2.5	2.6			00AH03								
00AH03a	gabbro							00AH03a	536.00	366.33	538.67	3.16	3.13	3.11		
00AH04	gabbro	low, dead	2.91	0.15				00AH04								
00AH04a	gabbro							00AH04a	693.40	467.11	697.16	3.06	3.03	3.01		
00AH05	gabbro	med	24.3	33.2				00AH05	636.70	423.31	639.41	2.98	2.96	2.95		
00AH06	gabbro	high	113	96.6				00AH06	272.10	182.77	273.20	3.05	3.02	3.01		
00AH07(1)	gabbro	high, med	45.6	89.6	90.9			00AH07(1)								
00AH07(2)	gabbro	high	93.7					00AH07(2)								
00AH08	gabbro	med, low	11.2	5.17	60.4			00AH08	324.70	218.37	326.11	3.05	3.03	3.01		
00AH10	gabbro	med, low	14	69.2				00AH10	450.10	302.23	453.20	3.04	3.00	2.98		
00AH13	gabbro	med, low	29.1	6.9	2.19			00AH13								
00AH13a	gabbro							00AH13a	894.76	607.02	898.30	3.11	3.08	3.07		
00AH13b	gabbro							00AH13b	285.42	189.65	287.01	2.98	2.95	2.93		
00AH13c	gabbro							00AH13c	261.65	180.77	262.11	3.24	3.22	3.22		
00AH13d	gabbro							00AH13d	553.75	378.33	555.07	3.16	3.14	3.13		
00AH13himag	gabbro	high	87.3					00AH13himag								
00AH14	gabbro	med	40.7	44.1				00AH14								
00AH14	gabbro	high,med	85.8	10.7				00AH14								
00AH14c	gabbro							00AH14c	210.16	142.13	211.04	3.09	3.06	3.05		
00AH15b	gabbro							00AH15b	505.78	339.11	507.81	3.03	3.01	3.00		
00AH21	gabbro	med, low	3.59	26.8				00AH21	583.04	378.49	586.30	2.85	2.82	2.81		
00AH21	gabbro	med, low	9.09	6.33	30.6			00AH21								
00AH25a	gabbro							00AH25a	650.11	443.55	650.72	3.15	3.14	3.14		
00AH26	gabbro	low,dead	0.22	3.51				00AH26	851.44	563.57	854.00	2.96	2.94	2.93		
00AH28	gabbro	med	34.6	37.8				00AH28	446.86	305.36	467.96	3.16	2.88	2.75		
00Mv08	gabbro	med	38.6					00Mv08								
00Mv09	gabbro	high	93.7	109			gabbro	00Mv09							gabbro	
00AH07	gabbro					ave	37.40	00AH07	823.35	560.90	825.47	3.14	3.12	3.11	3.03	ave
00AH02	gabbro & dunite	dead	0.24	0.2		stddev	35.47	00AH02							0.10	std dev
00AH16A(1)	gabbro & mafic	med, dead	27.5	0.51		count	41	00AH16A(1)							20	count
00AH16A(2)	gabbro & mafic	low,dead	3.13	0.1		max	113	00AH16A(2)								
00AH16Axtra	gabbro & mafic	low,dead	12.6	0.85		min	0	00AH16Axtra								
00AH16B	gabbro & mafic	low, dead	1.53	0.42	4.08			00AH16B								
00AH15	gabbro & umafic	med	45.2	35.4				00AH15								
00AH15big	gabbro & umafic	high	63.7	57.8				00AH15big								
00AH15himag	gabbro & umafic	high	91					00AH15himag								
00Mv04	gabbro cumulate	low	6.22	4.08				00Mv04	372.48	259.21	373.35	3.29	3.27	3.26		
00AH17	gabbro metamophic	med, low	24.7	2.05				00AH17								
00Mv20	gabbro peroxenite	med	13.7	39.7	41.9			00Mv20	439.45	296.58	441.22	3.08	3.05	3.04		
00Mv03	gabbro serpentine	low	9.92	3.14				00Mv03	734.20	508.79	735.97	3.26	3.24	3.23		
00AH11	gabbro(?)	low	16	6.81				00AH11	645.30	443.73	647.25	3.20	3.18	3.17		
00Mv07	mafic	low	6.16					00Mv07								
00Mv16	mafic igneous	dead	0.34					00Mv16								
00Mv01	mafic schistose	med,low	6.14	11	28.5			00Mv01								
00Mv02	mafic schistose	med,low	11	6.14	28.5			00Mv02								
00Mv03	SW Asik Mtn	dead	0.11	0				00Mv03								
00AH01A	umafic	med, low	5.05	24	2.99	49.1		00AH01A	430.45	287.68	431.60	3.01	3.00	2.99		
00AH01B	umafic							00AH01B	694.10	481.82	696.81	3.27	3.24	3.23		
00AH03b	umafic							00AH03b	345.80	236.57	347.54	3.17	3.13	3.12		
00AH12	umafic	low	3.02	2.23				00AH12	494.80	341.81	496.27	3.23	3.21	3.20		
00AH14b	umafic							00AH14b	352.76	244.36	354.33	3.25	3.22	3.21		
00AH15a	umafic							00AH15a	506.70	350.92	509.25	3.25	3.22	3.20		
00AH25b	umafic						umafic	00AH25b	195.49	135.60	196.18	3.26	3.24	3.23	umafic	
00AH04b	umafic or pyx-gabbro					ave	14.40	00AH04b	399.90	274.08	401.27	3.18	3.15	3.14	3.18	ave
00Mv05	W. Asik Mtn	dead	0.6			stddev	18.93	00Mv05							0.08	std dev
						count	6								8	count

Table 2.1

Creek bottom susceptibility measurements - Noatak Quad, Alaska, 15 June 2000
Rick Saltus and Travis Hudson

Site #1 (also AH22)

LON	-162.1801
LAT	67.7441
ELEV (ft)	875

Susceptibilities (SI x 10-3)

	20	7	13	0.6	
	13	32	0.3	43	
	1	13	0.5	54	
	0.4	4	26	13	
	0.4	0.6	0.4	45	
	0.4	0.6	11	19	
	6	0.5	19	0.7	
	0.6	11	0.4	0.7	
	0.3	11	0.5	49	
	8	0.8	10	22	
	10	0.8	27	0.8	
	5	0.6	5	0.7	
	20	0.7	0.9	2	
	6	4	1	8	
	0.4	38	0.6	14	
	4	0.5	0.5	3	
	1	16	0.7	0.8	
	29	0.9	28	4	
	52	2	17	4	
	32	1	0.6	0.8	
	3	0.9	4	4	
	23	23	6	0.8	
	0.4	0.8	15	13	
	9	0.9	16	0.7	
	33	48	1	0.9	
Average	11.1	8.7	8.2	12.2	10.1
Std dev	13.6	13.1	9.4	17.1	13.5
Median	6	1	4	4	4
Geomean	3.9	2.8	2.9	4.0	3.3

Histogram bins
5
10
20
30
40
50
60
70

Bin	*Frequency*
5	57
10	9
20	17
30	7
40	4
50	4
60	2
70	0
More	0

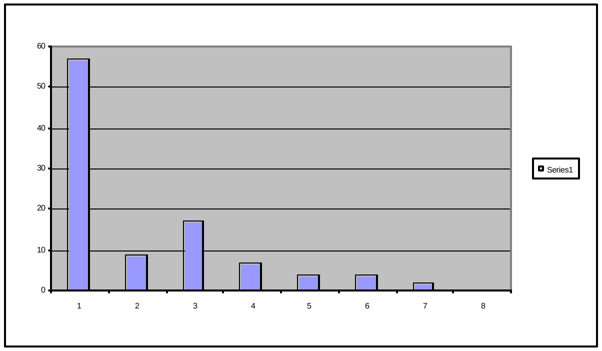

Table 2.2

Creek bottom susceptibility measurements - Noatak Quad, Alaska, 15 June 2000
Rick Saltus and Travis Hudson

Site #2 (also AH23)	
LON	-162.1442
LAT	67.7753
ELEV (ft)	900

Susceptibilities (SI x 10-3)

	15	36	0.9	10	
	80	2	2	18	
	1	1	44	87	
	0.5	26	53	21	
	66	1	1.7	23	
	65	47	2	26	
	12	6	32	2	
	21	32	71	3	
	7	0.6	0.7	40	
	3	0.4	16	3	
	47	5	0.5	4	
	1	12	94	0.6	
	37	25	0.6	10	
	39	7	12	9	
	36	43	93	0.5	
	32	69	83	19	
	68	1	25	3	
	47	7	5	20	
	53	20	0.6	8	
	25	4	40	33	
	10	5	2	20	
	5	0.8	2	59	
	1	37	1	0.7	
	17	106	22	2	
	106	0.4	5	52	
Average	31.8	19.8	24.4	19.0	23.7
Std dev	28.8	25.8	31.3	21.4	27.2
Median	25	7	5	10	12
Geomean	15.3	6.7	7.0	8.8	8.9

Histogram bins

5
10
20
30
40
50
60
70

Bin	*Frequency*
5	39
10	9
20	11
30	9
40	11
50	5
60	4
70	4
More	8

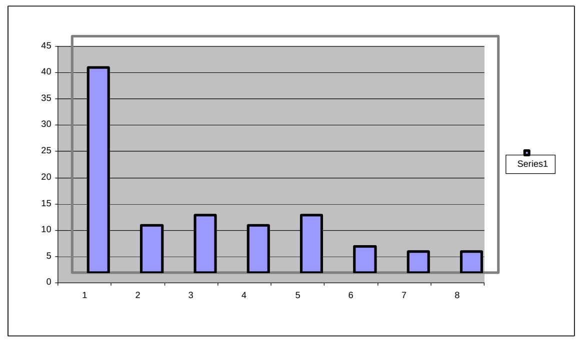

Table 2.3

Creek bottom susceptibility measurements - Noatak Quad, Alaska, 15 June 2000
Rick Saltus and Travis Hudson

Site #3 (also AH24)

LON	-162.0826
LAT	67.8039
ELEV (ft)	900

Susceptibilities (SI x 10-3)

	11	38	23	0.9	
	30	26	0.1	11	
	0.5	23	28	45	
	18	15	0.8	24	
	3	8	31	32	
	14	34	2	2	
	24	22	27	23	
	2	27	4	14	
	0.1	0.3	11	70	
	34	25	13	8	
	0.1	10	3	1	
	3	39	4	0.3	
	24	39	37	7	
	23	36	30	12	
	0.7	71	0.4	47	
	21	8	27	23	
	17	20	33	33	
	3	0.7	22	45	
	0.2	3	10	0.9	
	0.3	11	7	1	
	7	0.02	6	28	
	8	9	26	3	
	8	4	12	15	
	0.2	8	0.1	13	
	17	40	6	2	
Average	10.8	20.7	14.5	18.4	16.1
Std dev	10.6	17.2	12.4	18.5	15.3
Median	8	20	11	13	11.5
Geomean	3.8	10.1	6.7	8.4	6.8

Histogram bins
5
10
20
30
40
50
60
70

Bin	*Frequency*
5	32
10	14
20	16
30	21
40	12
50	3
60	0
70	1
More	1

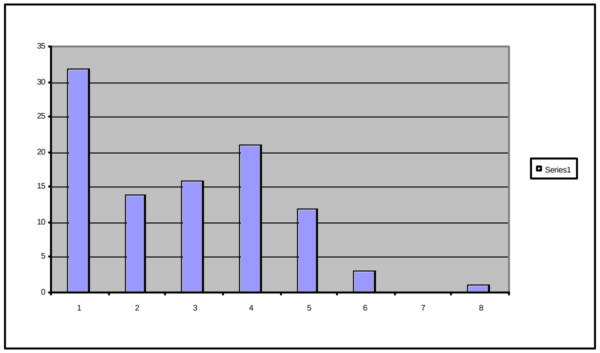

Table 2.4

Creek bottom susceptibility measurements - Noatak Quad, Alaska, 15 June 2000
Rick Saltus and Travis Hudson

Site #4 (also AH25)

LON	-162.0051
LAT	67.7966
ELEV (ft)	940

Susceptibilities (SI x 10-3)

	14	17	1	16	
	2	7	11	2	
	41	31	20	12	
	4	5	7	101	
	14	11	19	12	
	26	17	14	8	
	0.9	55	28	16	
	3	30	26	13	
	1	24	2	31	
	45	1	8	22	
	6	36	1	17	
	38	1	29	32	
	4	9	1	35	
	18	5	1	21	
	14	1	17	3	
	2	35	87	12	
	0.6	21	34	16	
	3	1	1	11	
	43	21	7	24	
	10	21	3	7	
	24	1	1	20	
	3	2	40	2	
	18	30	14	9	
	8	15	4	28	
	37	3	48	14	
Average	15.2	16.0	17.0	19.4	16.9
Std dev	15.0	14.3	19.9	19.3	17.1
Median	10	15	11	16	14
Geomean	7.9	8.5	7.7	13.8	9.2

Histogram bins
5
10
20
30
40
50
60
70

Bin	*Frequency*
5	31
10	11
20	26
30	15
40	10
50	4
60	1
70	0
More	2

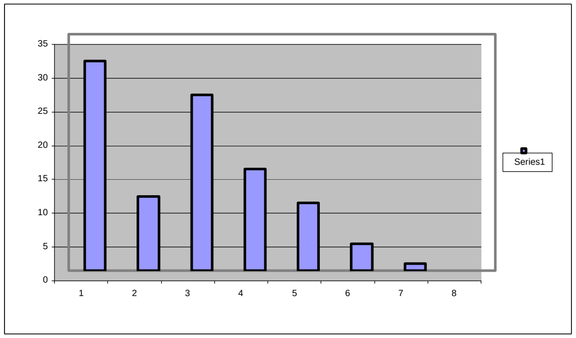

Table 2.5

Creek bottom susceptibility measurements - Noatak Quad, Alaska, 15 June 2000
Rick Saltus and Travis Hudson

Site #5 (also AH26)

LON	-161.9877
LAT	67.7756
ELEV (ft)	1050

Susceptibilities (SI x 10-3)

	5	0.4	30	22	
	0.3	30	1	20	
	15	13	13	4	
	0.6	59	31	4	
	42	49	31	0.1	
	22	14	12	10	
	17	3	25	4	
	34	28	1	9	
	29	10	4	3	
	23	26	14	12	
	16	2	18	37	
	31	26	17	36	
	24	1	23	20	
	19	0.3	0.1	0.3	
	13	0.8	29	8	
	29	12	27	31	
	14	45	25	25	
	39	0.3	47	48	
	57	36	15	32	
	1	8	30	6	
	37	0.1	2	12	
	12	18	52	17	
	34	22	37	20	
	10	38	1	20	
	33	45	15	23	
Average	22.3	19.5	20.0	16.9	19.7
Std dev	14.3	17.9	14.4	12.8	14.9
Median	22	14	18	17	18
Geomean	14.2	7.4	11.0	9.9	10.3

Histogram bins
5
10
20
30
40
50
60
70

Bin	*Frequency*
5	24
10	7
20	25
30	20
40	15
50	6
60	3
70	0
More	0

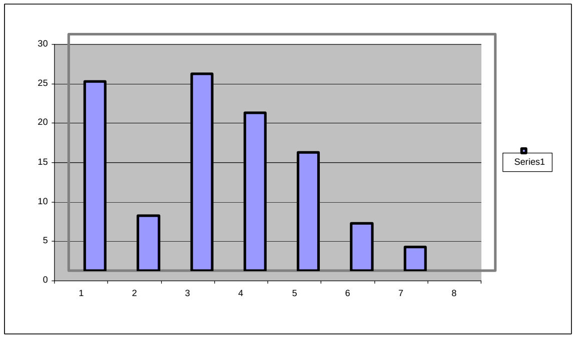

Table 2.6

Creek bottom susceptibility measurements - Noatak Quad, Alaska, 15 June 2000
Rick Saltus and Travis Hudson

Site #6 (also AH27)

LON	-162.0347
LAT	67.7556
ELEV (ft)	1250

Susceptibilities (SI x 10-3)

	25	26	3	1	
	0.7	0.6	16	0.8	
	6	0.6	0.9	32	
	0.6	0.9	18	1	
	0.5	1	1	19	
	9	1	21	3	
	0.5	1	0.9	1	
	14	8	0.9	0.9	
	0.6	33	15	0.9	
	0.5	0.8	13	3	
	0.5	0.8	38	3	
	0.6	20	1	1	
	1	12	9	10	
	6	1	9	1	
	24	7	11	29	
	1	1	30	1	
	0.4	2	2	1	
	10	6	1	21	
	0.8	5	1	19	
	0.8	6	20	4	
	4	11	50	3	
	7	7	10	29	
	28	28	7	1	
	0.6	9	1	1	
	0.6	0.7	10	4	
Average	5.7	7.6	11.6	7.6	8.1
Std dev	8.4	9.4	12.7	10.4	10.4
Median	0.8	5	9	3	3
Geomean	2.0	3.3	5.5	3.1	3.2

Histogram bins
5
10
20
30
40
50
60
70

Bin	*Frequency*
5	57
10	17
20	12
30	10
40	3
50	1
60	0
70	0
More	0

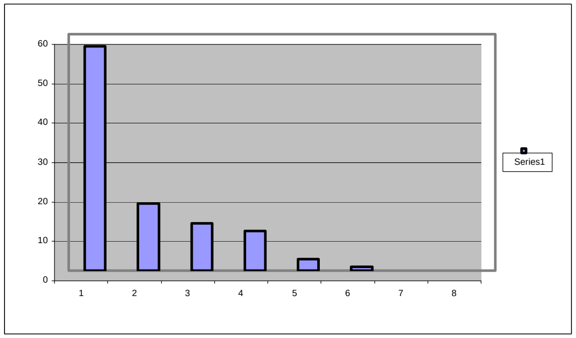

Table 2.7

Creek bottom susceptibility measurements - Noatak Quad, Alaska, 15 June 2000
Rick Saltus and Travis Hudson

Site #7 (also AH28)

LON	-162.0930
LAT	67.7123
ELEV (ft)	950

Susceptibilities (SI x 10-3)

	6	0.1	30	10	
	1	35	37	0.4	
	3	14	24	0.2	
	0.5	19	0.1	5	
	3	7	4	28	
	27	0.7	51	14	
	6	0.9	24	42	
	4	28	5	5	
	98	0.9	0.1	35	
	0.9	11	0.4	0.4	
	0.4	20	5	0.2	
	0.5	3	0.2	7	
	0.2	12	31	15	
	0.4	1	0.5	3	
	0.1	11	29	13	
	38	1	24	0.3	
	0.5	0.7	15	30	
	24	19	0.4	2	
	6	0.2	19	7	
	16	27	0.3	12	
	3	0.3	0.5	0.1	
	1	0.1	20	0.1	
	7	14	1	17	
	0.2	34	0.4	25	
	0.9	0.1	1	0.2	
Average	9.9	10.4	12.9	10.9	11.0
Std dev	20.8	11.5	14.8	12.3	15.1
Median	3	7	5	7	4.5
Geomean	2.2	3.0	3.2	3.2	2.9

Histogram bins
5
10
20
30
40
50
60
70

Bin	*Frequency*
5	54
10	8
20	17
30	12
40	6
50	1
60	1
70	0
More	1

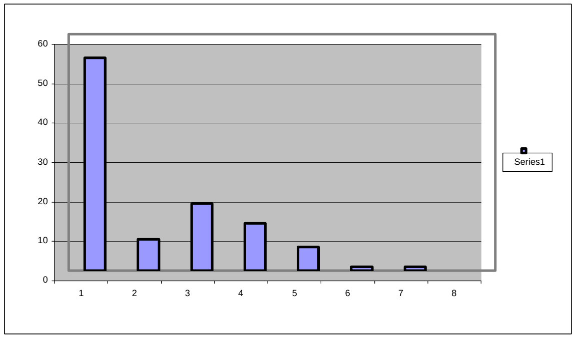

Table 3 - Physical property measurements
Format: AVERAGE±STD DEV(#SAMPLES)

DENSITY (gm/cm^3)			
	basalt	gabbro	umafic
Noatak	2.85±0.09(4)	3.03±0.10(20)	3.18±0.08(8)
Siniktanneyak	2.74±0.12(7)	2.91±0.08(13)	2.96±0.17(4)

SUSCEPT (SI x 10-3)			
	basalt	gabbro	umafic
Noatak	15.5±27.2(12)	37.4±35.5(41)	14.4±18.9(6)
Maiyumerak	15.1±16.2(700)		
Siniktanneyak	2.3±5.6(7)	9.1±13.4(13)	2.39±2.1(4)
Sue Karl rx	2.1±2.9(5)	0.6±0.7(8)	

EXPLANATION

Noatak = Hand samples collected and measured by Saltus and Hudson (see Table 1)
Maiyumerak = Field measurements by Saltus and Hudson (see Table 2)
Siniktanneyak = Hand samples collected and measured by Morin
Sue Karl rx = Baird Mountains samples collected by Sue Karl,
susceptibilities measured by Saltus

FIGURE G1 - Thin layer magnetic models along profile #1.

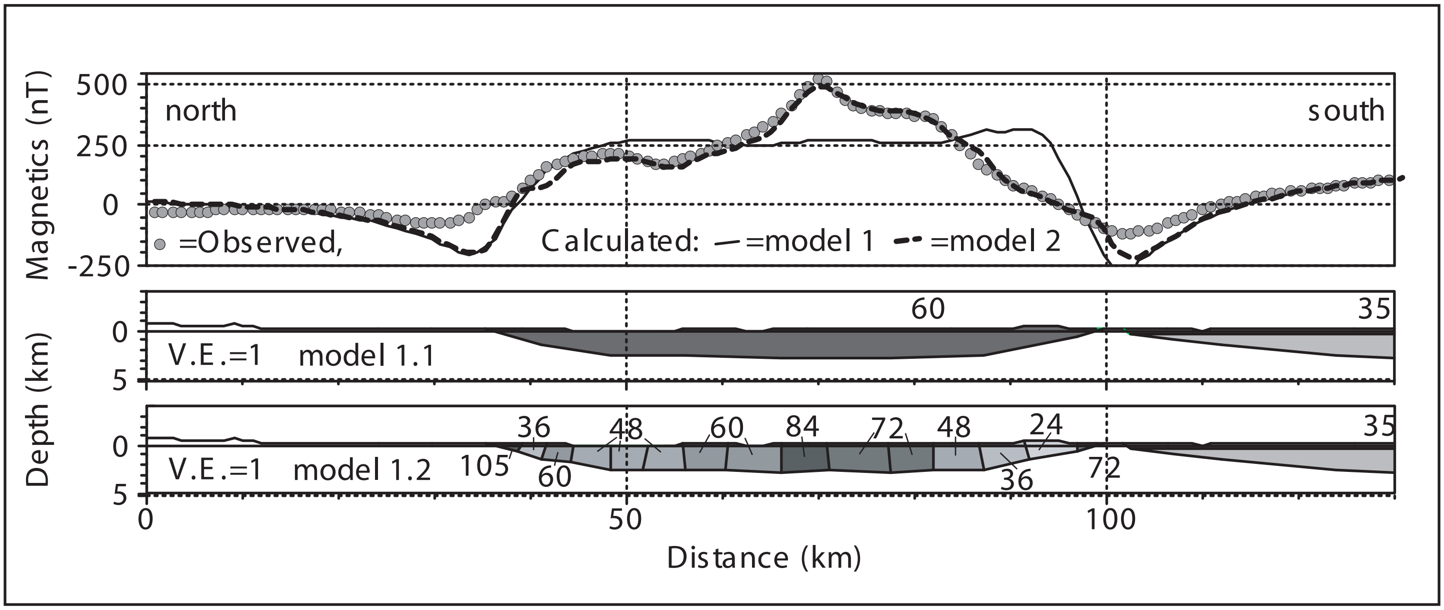

FIGURE G2 - Uniformly magnetized body models along profile #2.

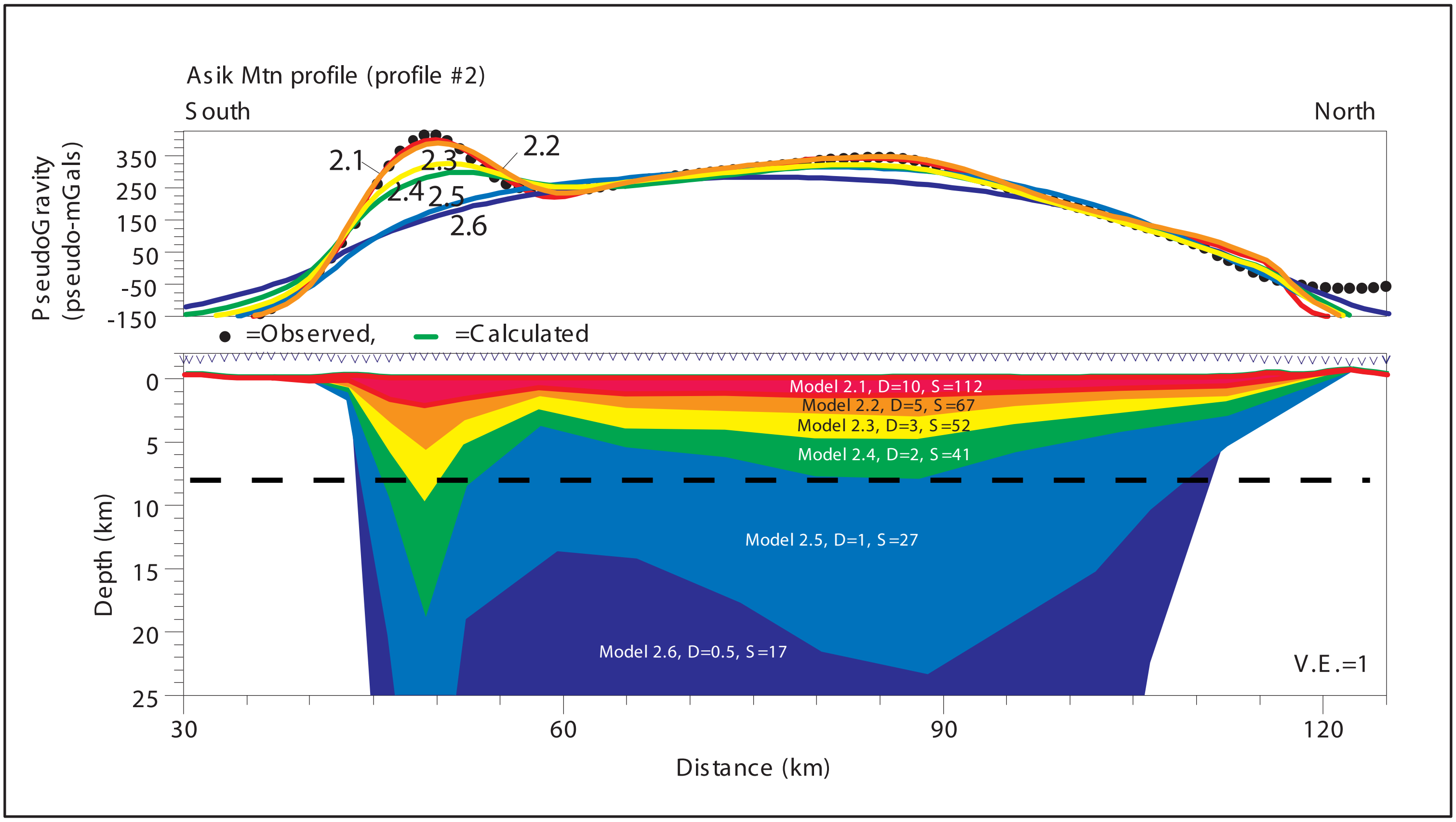

Figure G3 - Two-body models along profile #1

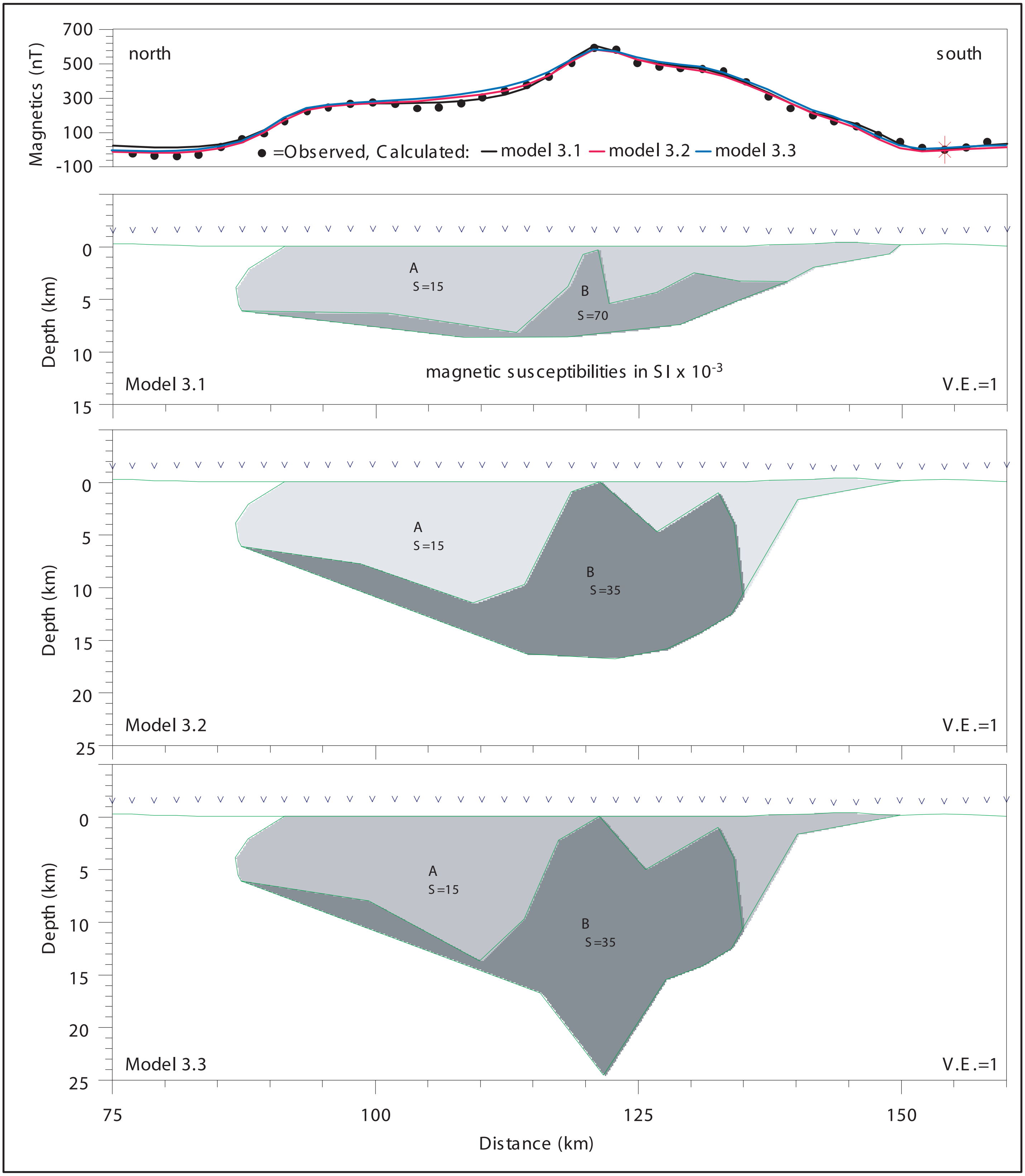

Figure G4 - Multi-body magnetic and gravity models along profile #2